PHYSICAL REVIEW D **95,** 035041 (2017)

Top and bottom tensor couplings from a color octet scalar

Roberto Martinez[1,*] and German Valencia[2,†]

[1]*Departamento de Física, Universidad Nacional de Colombia, Ciudad Universitaria, K. 45 No. 26-85, Bogotá D.C. 11001, Colombia*

[2]*School of Physics and Astronomy, Monash University, Wellington Road, Melbourne, Victoria 3800, Australia*

(Received 11 December 2016; published 28 February 2017)

We compute the one-loop contributions from a color octet scalar to the tensor anomalous couplings of top and bottom quarks to gluons, photons and W bosons. We use known constraints on the parameters of the model to compare the predicted size of these couplings with existing phenomenological constraints.

DOI: 10.1103/PhysRevD.95.035041

I. INTRODUCTION

One of the main tasks of the LHC is to measure the couplings between quarks and gauge bosons precisely in order to search for new physics through possible deviations from their standard model (SM) values. All the possible deviations from the SM couplings have been catalogued up to dimension six with an effective Lagrangian that is consistent with the symmetries of the SM [1,2]. Of particular interest are the couplings of the top-quark because many ideas for new physics stem from the large value of its mass, and its couplings can be probed by the LHC which is the first top-quark factory. Related bottom-quark couplings may also receive large corrections in models where top-quark couplings are enhanced.

Amongst the anomalous top-quark couplings one finds the flavor diagonal dipole-type couplings to photons and gluons. These are simply the anomalous magnetic moment (MDM), the electric dipole moment (EDM), and their color generalizations CMDM and CEDM, respectively. These couplings introduce spin correlations between top and antitop pairs beyond those present in the SM, and have thus received much attention because the weak decay of the top-quark allows one to analyze its spin. They are usually parametrized as.[1]

$$\mathcal{L} = \frac{e}{2}\bar{f}\sigma^{\mu\nu}(a_f^\gamma + i\gamma_5 d_f^\gamma)fF_{\mu\nu} + \frac{g_s}{2}\bar{f}T^a\sigma^{\mu\nu}(a_f^g + i\gamma_5 d_f^g)fG^a_{\mu\nu}. \quad (1)$$

LHC related phenomenological studies have illustrated possible constraints on these couplings proposing a variety of observables: deviations from SM cross sections [4,5], triple product ('T-odd') correlations [6–13], new CP-even spin correlations [14,15], lepton energy asymmetries [16], and associated production of Higgs bosons [17]. The bottom-quark CEDM and CMDM couplings have been studied in associated production with a Higgs boson [17,18]. To study the photon couplings, rare decays such as $B \to X_s\gamma$, as well as $t\bar{t}\gamma$ cross sections have been proposed [19].

A related set of anomalous couplings, the transition dipole moments $f_T^{L,R}$, occurs in the charged coupling tbW

$$\mathcal{L}_{tbW} = \frac{g}{\sqrt{2}}\bar{b}\gamma^\mu(f_V^L P_L + f_V^R P_R)tW_\mu^- - \frac{g}{\sqrt{2}}\bar{b}\frac{\sigma^{\mu\nu}\partial_\nu W_\mu^-}{M_W}(f_T^L P_L + f_T^R P_R)t + \text{H.c.} \quad (2)$$

LHC related phenomenological studies for these couplings also exist, for example the study of W helicity fractions and angular asymmetries [20–22] as well as T-odd observables [23–25]. Recent overviews of anomalous couplings in the top-quark and Higgs sectors can be found in Refs. [26–30].

The size of these anomalous couplings has been considered in a variety of cases: 331 models, topcolor models and extra dimension models [3]; two Higgs doublet models [3,31–35]; models with vector like multiplets [36]; and MSSM extensions [37]. Their one-loop value within the SM has also been computed in some cases [3,32], and it is known that the EDMs vanish at this order within the SM.

An interesting extension of the SM results from considering an additional color octet scalar, as introduced some time ago by Manohar and Wise (MW) [38]. This particular extension of the SM is motivated by the requirement of minimal flavor violation, with which new physics naturally satisfies constraints on flavor changing neutral currents [39,40]. In this paper we consider the contribution of the new scalars that appear in the MW model to the anomalous

*remartinezm@unal.edu.co

†On leave from Department of Physics, Iowa State University, Ames, IA 50011, USA.
German.Valencia@monash.edu

[1]In the notation of [3] $\Delta\kappa = 4m_t a_t^g$.

couplings described above. Since the couplings of these scalars to quarks are proportional to the quark masses, this model is an example where larger effects are expected for top and bottom anomalous couplings.

II. THE MODEL

The MW model contains a number of parameters that have been studied phenomenologically. In particular the new color octet scalars have a large effect on loop level Higgs production and decay [38]. They are also constrained by precision measurements [41,42], one-loop effective Higgs couplings [43–48], flavor physics [49,50], unitarity and vacuum stability [51–53] and other LHC processes [54–57].

In the MW model, the inclusion of the new field S transforming as $(8,2,1/2)$ under the SM gauge group $SU(3)_C \times SU(2)_L \times U(1)_Y$ introduces several new, renormalizable, interaction terms to the Lagrangian. Because S has nontrivial SM quantum numbers, it will have the corresponding gauge interactions. In addition there will be new terms in the Yukawa couplings that are consistent with minimal flavor violation [38],

$$\begin{aligned}\mathcal{L}_Y = &-\eta_U e^{i\alpha_U} g^U_{ij} \bar{u}_{Ri} T^a Q_j S^a \\ &- \eta_D e^{i\alpha_D} g^D_{ij} \bar{d}_{Ri} T^a Q_j S^{\dagger a} + \text{H.c}, \end{aligned} \tag{3}$$

where Q_i are left-handed quark doublets, $S = S^a T^a (a = 1,\ldots,8)$ and the $SU(3)$ generators are normalized as $\text{Tr}(T^a T^b) = \delta^{ab}/2$. The matrices $g^{U,D}_{ij}$ are the same as the quark Yukawa couplings, and $\eta_{U,D}$ along with their phases $e^{i\alpha_{U,D}}$, are new overall factors (that can be complex and we write the phases explicitly). Nonzero phases would signal CP violation beyond the SM and contribute to the EDM and CEDM of quarks. In the quark mass eigenstate basis these couplings are given by

$$\begin{aligned}\mathcal{L}_Y = &-\frac{\sqrt{2}}{v}\eta_U e^{i\alpha_U} \bar{U}_R T^a \hat{M}^u U_L S^{a0} \\ &+ \frac{\sqrt{2}}{v}\eta_U e^{i\alpha_U} \bar{U}_R T^a \hat{M}^u V_{KM} D_L S^{a+} \\ &- \frac{\sqrt{2}}{v}\eta_D e^{i\alpha_D} \bar{D}_R T^a \hat{M}^d D_L S^{a0\dagger} \\ &- \frac{\sqrt{2}}{v}\eta_D e^{i\alpha_D} \bar{D}_R T^a \hat{M}^u V^\dagger_{KM} U_L S^{a-} + \text{H.c.}, \end{aligned} \tag{4}$$

where $\hat{M}^{u,d}$ are the diagonal quark mass matrices, $\hat{M}^{u,d} = \text{diag}(m_{u,d}, m_{c,s}, m_{t,b})$; the quark fields are $U_{L,R} = \text{diag}(u_{L,R}, c_{L,R}, t_{L,R})$ and $D_{L,R} = \text{diag}(d_{L,R}, s_{L,R}, b_{L,B})$. The neutral complex field S^{a0} can be further decomposed into a scalar S^{a0}_R and a pseudoscalar S^{a0}_I as $S^{a0} = (S^{a0}_R + iS^{a0}_I)/\sqrt{2}$. The following combinations of constants usually appear together, and in our results we will use the shorthand:

$$g_t \equiv \left(\eta_U \frac{m_t}{v}\right), \qquad g_b \equiv \left(\eta_D \frac{m_b}{v}\right). \tag{5}$$

The most general renormalizable scalar potential for this model is given in Ref. [38] and contains many terms. Of these, our calculation will only depend on the terms contributing to the mass of the new scalars,

$$\begin{aligned}V = &\lambda\left(H^{\dagger i}H_i - \frac{v^2}{2}\right)^2 + 2m_S^2 \text{Tr} S^{\dagger i} S_i + \lambda_1 H^{\dagger i} H_i \text{Tr} S^{\dagger j} S_j \\ &+ \lambda_2 H^{\dagger i} H_j \text{Tr} S^{\dagger j} S_i + (\lambda_3 H^{\dagger i} H^{\dagger j} \text{Tr} S_i S_j . + \text{H.c.}) \end{aligned} \tag{6}$$

Here $v \sim 246$ GeV is the Higgs vacuum expectation value (vev) with $\langle H \rangle = v/\sqrt{2}$, the traces are over the color indices and the $SU(2)$ indices i, j are displayed explicitly. Furthermore, λ_3 can be chosen to be real by a suitable definition of S. After symmetry breaking, the nonzero vev of the Higgs gives the physical Higgs scalar h a mass $m_H^2 = 2\lambda v^2$ and it also splits the octet scalar masses as,

$$\begin{aligned} m^2_{S^\pm} &= m_S^2 + \lambda_1 \frac{v^2}{4}, \\ m^2_{S^0_{R,I}} &= m_S^2 + (\lambda_1 + \lambda_2 \pm 2\lambda_3)\frac{v^2}{4}. \end{aligned} \tag{7}$$

The parameters m_S^2, and $\lambda_{1,2,3}$ should be chosen such that the above squared masses remain positive. Relations between various parameters follow from custodial symmetry, and we will use $2\lambda_3 = \lambda_2$ which makes S_I and $S^\pm$ degenerate.

III. ANOMALOUS COUPLINGS

A. Top CMDM and CEDM

We begin with the dipole-type couplings of the top-quark to the gluon, the chromo magnetic dipole moment a_t^g and chromo electric dipole moment d_t^g in the notation of Eq. (1). In the one-loop calculation these couplings are finite since they do not appear in the tree-level Lagrangian and receive several contributions. One such contribution arises from loops involving neutral scalars as depicted in the two diagrams shown in Fig. 1. Denoting by M_S the mass of the corresponding scalar in the loop and using $r_{tR} = m_t/M_{S_R}$, $r_{tI} = m_t/M_{S_I}$, these two diagrams result in

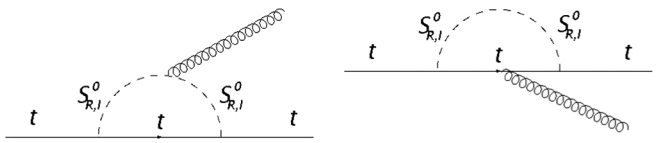

FIG. 1. Diagrams with neutral scalars contributing to $a^g_{t,b}$ and $d^g_{t,b}$ as described in the text.

$$a_t^g = \frac{m_t g_t^2}{16\pi^2 M_{S_R}^2}\left(\frac{3}{2}(F_{2,1}(r_{tR}) - 2c_U^2 F_{1,1}(r_{tR})) - \frac{1}{6}(F_{3,0}(r_{tR}) - 2c_U^2 F_{2,0}(r_{tR}))\right) + \frac{m_t g_t^2}{16\pi^2 M_{S_I}^2}\left(\frac{3}{2}(F_{2,1}(r_{tI}) - 2s_U^2 F_{1,1}(r_{tI})) - \frac{1}{6}(F_{3,0}(r_{tI}) - 2s_U^2 F_{2,0}(r_{tI}))\right)$$

$$d_t^g = \frac{s_U c_U m_t}{8\pi^2} g_t^2 \left[\frac{(\frac{3}{2}F_{1,1}(r_{tR}) - \frac{1}{6}F_{0,0}(r_{tR}))}{M_{S_R}^2} - \frac{(\frac{3}{2}F_{1,1}(r_{tI}) - \frac{1}{6}F_{0,0}(r_{tI}))}{M_{S_I}^2}\right]. \quad (8)$$

The factors $3/2$ and $-1/6$ are the color factors for the diagrams on the left and right respectively, and the form factors $F_{i,j}(r_t)$ are one parameter Feynman integrals explicitly given in the Appendix. We have also introduced the shorthand notation $c_U = \cos\alpha_U$, $s_U = \sin\alpha_U$.

There are also two diagrams with charged scalars and a bottom-quark in the loop as shown in Fig. 2, and they result in

$$a_t^g = -\frac{m_t|V_{tb}|^2}{16\pi^2 M_{S^+}^2}\left[(g_t^2 + g_b^2)\left(\frac{3}{2}G_{1,2}(r_t, r_b) - \frac{1}{6}G_{2,1}(r_t, r_b)\right) + 2\frac{m_b}{m_t} g_t g_b \cos(\alpha_D + \alpha_U) \times \left(\frac{3}{2}G_{1,1}(r_t, r_b) + \frac{1}{6}G_{2,0}(r_t, r_b)\right)\right]$$

$$d_t^g = -\frac{m_t|V_{tb}|^2}{16\pi^2 M_{S^+}^2} 2\frac{m_b}{m_t} g_t g_b \sin(\alpha_D + \alpha_U) \times \left(\frac{3}{2}G_{1,1}(r_t, r_b) - \frac{1}{6}G_{2,0}(r_t, r_b)\right) \quad (9)$$

where the factors $3/2$ and $-1/6$ are again the color factors for the diagrams on the left and right respectively and $G_{i,j}(r_1, r_2)$ are one parameter Feynman integrals also shown in the Appendix. In the limit $m_b \to 0$, Eq. (9) simplifies considerably, with d_t^g vanishing and a_t^g retaining a term proportional to the top-quark mass (cubed),

$$a_t^g \approx -\frac{m_t|V_{tb}|^2}{16\pi^2 M_{S^+}^2} g_t^2 \left(\frac{3}{2}G_{1,2}(r_t, 0) - \frac{1}{6}G_{2,1}(r_t, 0)\right). \quad (10)$$

To combine the diagrams to obtain the final result it is important to note that the two neutral resonances tend to cancel each other's contribution to CP violation [56], and in fact produce a vanishing CEDM when they have the same mass. To extract the leading behavior in the mass difference, we write the scalar masses in the custodial symmetry limit as

$$M_{S_R}^2 = M_S^2 + \frac{v^2}{2}\lambda_2, \qquad M_{S_I}^2 = M_{S^\pm}^2 \equiv M_S^2 \quad (11)$$

and work to leading order in λ_2. We can then add all the contributions neglecting m_b and setting $V_{tb} = 1$ to finally obtain

$$a_t^g = -\frac{7}{12}\frac{m_t \eta_U^2}{16\pi^2 v^2} r_t^2 f(r_t),$$

$$d_t^g = -\frac{m_t \eta_U^2}{16\pi^2 M_S^2}\lambda_2 s_U c_U r_t^2 g(r_t), \quad (12)$$

where the functions $f(r)$, $g(r)$ are combinations of one dimensional Feynman parameter integrals and we show their numerical value in Fig. 3.

B. Bottom CMDM and CEDM

Similar diagrams, with the roles of top and bottom-quarks interchanged, generate a_b^g and d_b^g. The two diagrams with neutral scalars in the loop also have a bottom-quark in the loop, and are proportional to m_b (cubed). Defining $r_{bR,I} = m_b/M_{S_{R,I}}$ these two diagrams give

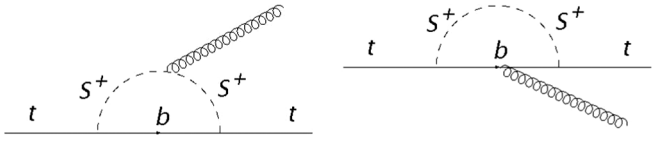

FIG. 2. Diagrams with charged scalars contributing to $a_{t,b}^g$ and $d_{t,b}^g$ as described in the text.

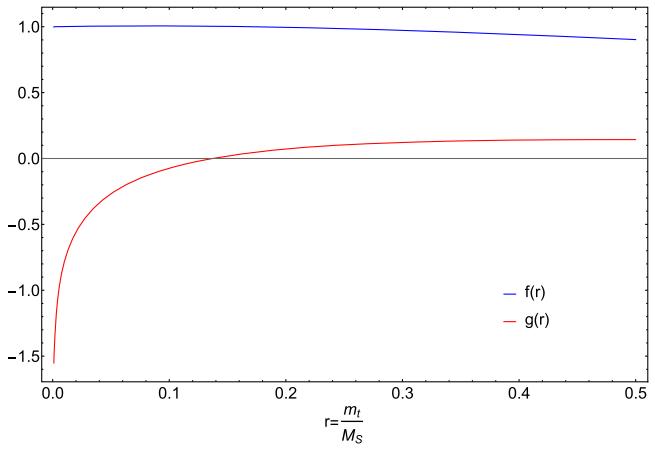

FIG. 3. Numerical evaluation of the functions $f(r)$ and $g(r)$ appearing in Eq. (12).

$$
\begin{aligned}
a_b^g &= \frac{m_b}{16\pi^2 M_{S_R}^2} g_b^2 \left(\frac{3}{2}(F_{2,1}(r_{bR}) - 2c_D^2 F_{1,1}(r_{bR})) - \frac{1}{6}(F_{3,0}(r_{bR}) - 2c_D^2 F_{2,0}(r_{bR}))\right) \\
&\quad + \frac{m_b}{16\pi^2 M_{S_I}^2} g_b^2 \left(\frac{3}{2}(F_{2,1}(r_{bI}) - 2s_D^2 F_{1,1}(r_{bI})) - \frac{1}{6}(F_{3,0}(r_{bI}) - 2s_D^2 F_{2,0}(r_{bI}))\right) \\
&\approx -\frac{7}{18}\frac{\eta_D^2 m_b}{16\pi^2 v^2} r_b^2 \\
d_b^g &= \frac{s_D c_D m_b}{8\pi^2} g_b^2 \left(\frac{(\frac{3}{2}F_{1,1}(r_{bR}) - \frac{1}{6}F_{0,0}(r_{bR}))}{M_{S_R}^2} - \frac{(\frac{3}{2}F_{1,1}(r_{bI}) - \frac{1}{6}F_{0,0}(r_{bI}))}{M_{S_I}^2}\right) \\
&\approx -\frac{\eta_D^2 m_b}{16\pi^2 M_S^2} c_D s_D \lambda_2 r_b^2 \left(\frac{3}{4} + \log\frac{m_b}{3M_S}\right),
\end{aligned} \tag{13}
$$

where we have used the shorthand notation $c_D = \cos\alpha_D$, $s_D = \sin\alpha_D$.

The two diagrams with charged scalars now have a top-quark in the loop and are analogous to Fig. 2 interchanging $t \leftrightarrow b$ and their corresponding couplings. The result can also be obtained with this substitution from Eq. (9), and in particular it contains terms enhanced by m_t^2/m_b^2 with respect to Eq. (13).

$$
\begin{aligned}
a_b^g &= -\frac{m_b|V_{tb}|^2}{16\pi^2 M_{S^+}^2}\left[(g_t^2 + g_b^2)\left(\frac{3}{2}G_{1,2}(r_b, r_t) - \frac{1}{6}G_{2,1}(r_b, r_t)\right)\right. \\
&\quad + 2\frac{m_t}{m_b} g_t g_b \cos(\alpha_D + \alpha_U) \\
&\quad \left.\times \left(\frac{3}{2}G_{1,1}(r_b, r_t) + \frac{1}{6}G_{2,0}(r_b, r_t)\right)\right] \\
d_b^g &= -\frac{m_t|V_{tb}|^2}{16\pi^2 M_{S^+}^2} 2 g_t g_b \sin(\alpha_D + \alpha_U) \\
&\quad \times \left(\frac{3}{2}G_{1,1}(r_b, r_t) - \frac{1}{6}G_{2,0}(r_b, r_t)\right).
\end{aligned} \tag{14}
$$

For regions of parameter space where $\eta_D m_b \ll \eta_U m_t$ we can ignore the contributions from neutral scalars in the loops and the complete result simplifies to

$$
\begin{aligned}
a_b^g &= -\frac{m_b|V_{tb}|^2}{16\pi^2 v^2} r_t^2 \left[\eta_U^2\left(\frac{3}{2}G_{1,2}(0, r_t) - \frac{1}{6}G_{2,1}(0, r_t)\right)\right. \\
&\quad + 2\eta_U\eta_D \cos(\alpha_D + \alpha_U) \\
&\quad \left.\times \left(\frac{3}{2}G_{1,1}(0, r_t) + \frac{1}{6}G_{2,0}(0, r_t)\right)\right] \\
d_b^g &= -\frac{m_b|V_{tb}|^2}{8\pi^2 v^2} r_t^2 \eta_U\eta_D \sin(\alpha_D + \alpha_U) \\
&\quad \times \left(\frac{3}{2}G_{1,1}(0, r_t) - \frac{1}{6}G_{2,0}(0, r_t)\right).
\end{aligned} \tag{15}
$$

The loop factors appearing in this result are evaluated numerically and plotted in Fig. 4. The second term in a_b^g dominates as long as $\eta_D/\eta_U \cos(\alpha_D + \alpha_U) \gtrsim 1/4$.

C. Anomalous magnetic and electric dipole moments

Once again these couplings are finite because they do not appear in the tree level Lagrangian. They can be extracted from our previous results by interpreting the wavy lines in the Feynman diagrams as photons: we only need to replace the color factor with the electric charge factor in the respective vertex. For neutral scalars and top-quarks in the loop the photon can only be emitted by the top-quark (diagram on the right in Fig. 1) and the result can be obtained from Eq. (8) by replacing the color factor $-1/6 g_s$ with the new color-electric charge factor $8/9e$. For the diagrams involving charged scalars in Fig. 2 we replace the color factors $3/2 g_s$ and $-1/6 g_s$ with $4/3e$ and $-4/9e$ respectively in Eq. (9). We obtain

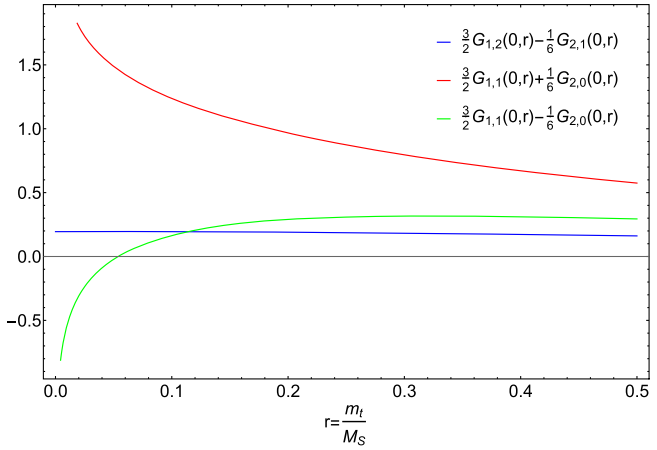

FIG. 4. Numerical evaluation of the functions appearing in Eq. (15).

$$a_t^\gamma = \frac{m_t g_t^2}{16\pi^2 M_{S_R}^2}\left(\frac{8}{9}(F_{3,0}(r_{tR}) - 2c_U^2 F_{2,0}(r_{tR}))\right) + \frac{m_t g_t^2}{16\pi^2 M_{S_I}^2}\left(\frac{8}{9}(F_{3,0}(r_{tI}) - 2s_U^2 F_{2,0}(r_{tI}))\right)$$
$$- \frac{m_t |V_{tb}|^2}{16\pi^2 M_{S^+}^2}\left[(g_t^2 + g_b^2)\left(\frac{4}{3}G_{1,2}(r_t, r_b) - \frac{4}{9}G_{2,1}(r_t, r_b)\right) + 2\frac{m_b}{m_t} g_t g_b \cos(\alpha_D + \alpha_U)\left(\frac{4}{3}G_{1,1}(r_t, r_b) + \frac{4}{9}G_{2,0}(r_t, r_b)\right)\right]$$
$$d_t^\gamma = \frac{s_U c_U m_t}{8\pi^2} g_t^2 \frac{8}{9}\left(\frac{F_{0,0}(r_{tR})}{M_{S_R}^2} - \frac{F_{0,0}(r_{tI})}{M_{S_I}^2}\right) - \frac{m_t |V_{tb}|^2}{16\pi^2 M_{S^+}^2} 2\frac{m_b}{m_t} g_t g_b \sin(\alpha_D + \alpha_U)\left(\frac{4}{3}G_{1,1}(r_t, r_b) - \frac{4}{9}G_{2,0}(r_t, r_b)\right). \quad (16)$$

To leading order in m_b and $\lambda_2 v^2/M_S^2$ and setting $V_{tb} = 1$, these simplify to

$$a_t^\gamma = -\frac{\eta_U^2 m_t}{9\pi^2 v^2} r_t^2\left(F_{2,1}(r_t) + \frac{3}{4}G_{1,2}(r_t, 0) - \frac{1}{4}G_{2,1}(r_t, 0)\right)$$
$$d_t^\gamma = -\frac{\eta_U^2 s_U c_U m_t}{18\pi^2 M_S^2}\lambda_2 r_t^2 F_{0,0}(r_t). \quad (17)$$

The loop factors appearing in this result are evaluated numerically and plotted in Fig. 5, with $V_{tb} = 1$, and $F_{0,0}$ scaled by a factor of 9 for convenience.

Similarly, for the MDM and EDM of the bottom quark, only the diagram to the right in Fig. 1 contributes and the result can be obtained by replacing $-1/6g_s$ with $-4/9e$ in Eq. (13). The resulting contributions are proportional to m_b^3 and negligible compared to those due to the exchange of a charged scalar. For the latter case the result follows from Eq. (14) replacing the color factors $3/2g_s$ and $-1/6g_s$ with $-4/3e$ and $8/9e$ respectively. Keeping only the leading terms in m_b we find,

$$a_b^\gamma = -\frac{m_b |V_{tb}|^2}{16\pi^2 v^2} r_t^2\left[\eta_U^2\left(-\frac{4}{3}G_{1,2}(r_b, r_t) + \frac{8}{9}G_{2,1}(r_b, r_t)\right)\right.$$
$$+ 2\eta_U\eta_D\cos(\alpha_D + \alpha_U)$$
$$\left.\times\left(-\frac{4}{3}G_{1,1}(r_b, r_t) - \frac{8}{9}G_{2,0}(r_b, r_t)\right)\right]$$
$$d_b^\gamma = -\frac{m_b |V_{tb}|^2}{8\pi^2 v^2} r_t^2 \eta_U\eta_D \sin(\alpha_D + \alpha_U)$$
$$\times\left(-\frac{4}{3}G_{1,1}(r_b, r_t) + \frac{8}{9}G_{2,0}(r_b, r_t)\right). \quad (18)$$

The loop factors appearing in this result are evaluated numerically and plotted in Fig. 6. From the figure we see that a_b^γ is dominated by the second term in the expression given in Eq. (18) as long as $\eta_D/\eta_U \cos(\alpha_D + \alpha_U) \gtrsim 1/4$.

D. *tbW* couplings

The MW model contributes to all the couplings that appear in Eq. (2), but we concentrate of the tensor couplings which are finite. The contribution to f_V^R is also finite and very interesting, but in this model it is suppressed by factors of m_b. We begin with the Feynman diagrams shown in Fig. 7. The diagrams to the left, one with S_R^0 and one with S_I^0, combine to yield the finite result (in this case the color factor is 4/3),

$$f_T^R = -\frac{1}{12\pi^2}\left(\eta_U\frac{m_t}{v}\right)^2 V_{tb} r_t^2 r_W e^{-2i\alpha_U} F_c(r_t, r_W) \quad (19)$$

where we have defined $r_t = m_t/M_S$ as before and $r_W = m_W/m_t$. The loop factor is written in the

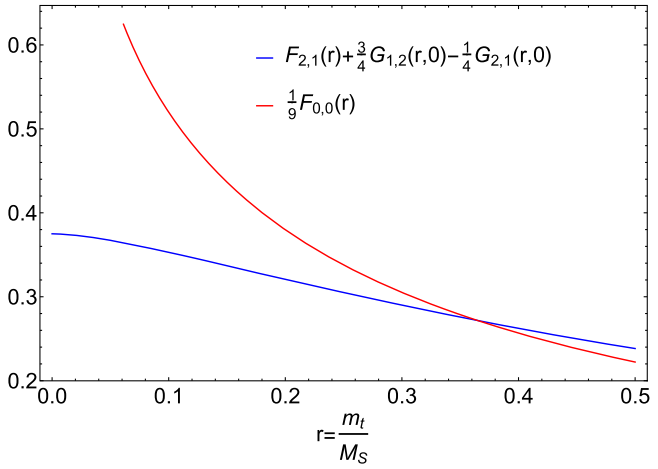

FIG. 5. Numerical evaluation of the functions appearing in Eq. (17).

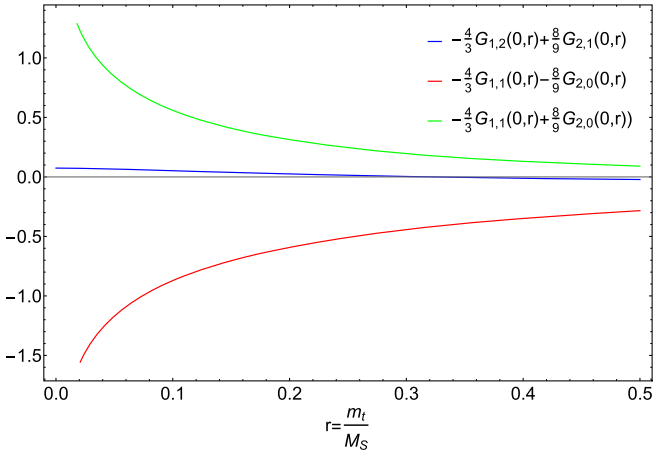

FIG. 6. Numerical evaluation of the functions appearing in Eq. (18).

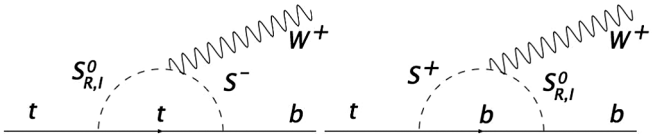

FIG. 7. Generic Feynman diagram contributing to f_T^R as described in the text.

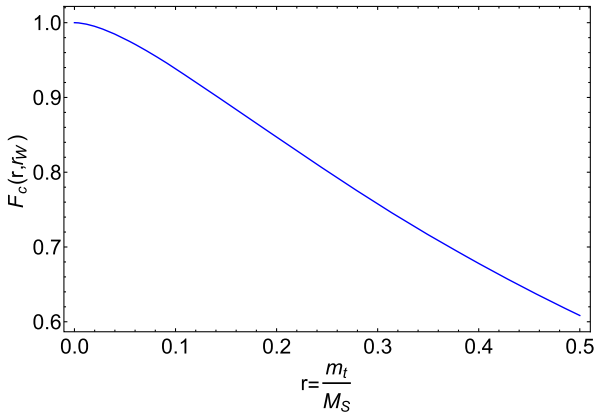

FIG. 8. Numerical evaluation of the function $F_c(r, r_W)$ appearing in Eq. (A3) for a fixed value of $r_W = m_W/m_t$.

Appendix in Eq. (A3), it satisfies $F_c(0, r_W) = 1$ and the r_t dependence is evaluated numerically and shown in Fig. 8. The diagrams also induce a nonzero f_T^L but it is proportional to m_b and we have dropped these terms for simplicity. Interestingly, these two diagrams also contribute to the form factor f_V^L (without an m_b suppression) as inferred from the Gordon decomposition of the result [proportional to $(p_t + p_b)^\mu \bar{b} P_R t$]. The form factor f_V^L, however, receives other contributions from these two diagrams and from additional diagrams, some of which are divergent. It is necessary to perform a full one-loop calculation, including renormalization, to obtain a finite result for f_V^L.

Diagrams to the right in Fig. 7, with the charged and neutral scalars interchanged are suppressed by at least m_b^2/m_t^2 with respect to Eq. (19) and are therefore negligible except for scenarios with $\eta_D \gg \eta_U$. Similarly, diagrams in which the W boson is emitted from the quark line contain an $S_{R,I}^0 b\bar{b}$ coupling and are also suppressed by m_b^2/m_t^2 with respect to Eq. (19).

IV. SUMMARY OF RESULTS AND COMPARISON WITH EXISTING CONSTRAINTS

There exist a number of phenomenological papers investigating possible constraints on these anomalous couplings. We collect some of these results in Table I.

In addition, the couplings in the tbW vertex have been recently constrained experimentally, with the 95% C.L. results from CMS being [63],

TABLE I. Summary of phenomenological constraints from different processes. LHC cross sections assume these can be measured to within the 1σ uncertainty of the NLO SM calculations. LHC asymmetries are simulations at LHC14 with 10 fb^{-1}. Bounds quoted are 1σ unless otherwise noted.

Process	Constraint
$\sigma(t\bar{t})$ [17]	$-0.029 \lesssim m_t a_t^g \lesssim 0.024$, $\lvert m_t d_t^g\rvert \lesssim 0.1$
$(t\bar{t})$ T-odd [17]	$\lvert m_t d_t^g\rvert \lesssim 0.009$
$\sigma(t\bar{t}h)$ [17]	$-0.016 \lesssim m_t a_t^g \lesssim 0.008$, $\lvert m_t d_t^g\rvert \lesssim 0.02$
neutron edm [58]	$m_t d_t^g < 2 \times 10^{-3}$ (indirect)
$\sigma(b\bar{b}h)$ [17]	$-1.3 \times 10^{-4} \lesssim m_b a_b^g \lesssim 2.4 \times 10^{-4}$ $\lvert m_b d_b^g\rvert \lesssim 1.7 \times 10^{-4}$
$B \to X_s\gamma$ [59]	$-0.15 < f_T^R < 0.57$ (95% C.L.)
$t \to bW$ helicity fractions [23]	$-0.0260 < f_T^R < 0.0312$ (2σ), $f_T^L = f_V^R = 0$
$t \to bW$ T-odd [23]	$\lvert\mathrm{Im}(f_T^R)\rvert \le 0.115$ (3σ), $f_T^L = f_V^R = 0$
$t \to bW$ asymmetries [23]	$\lvert\mathrm{Re}(f_T^R)\rvert \le 0.056$ (3σ), $f_T^L = f_V^R = 0$
$B \to X_s\gamma$ and $\sigma(t\bar{t}\gamma)$ [19]	$-1 \le m_t a_t^\gamma \le 0.15$, $-0.25 \le m_t d_t^\gamma \le 0.75$
R_b [60]	$-0.2 \le m_t a_t^\gamma \le 0.33$
8 parameter fit to LHC data [61,62]	$\lvert\mathrm{Re}(f_T^R)\rvert \le 0.120$, $\lvert\mathrm{Im}(f_T^R)\rvert \le 0.120$

$$|f_V^L| > 0.98, \qquad |f_V^R| < 0.16$$
$$|f_T^L| < 0.057, \qquad -0.049 < f_T^R < 0.048. \tag{20}$$

A search for CP violation has also been started by CMS but they have not yet constrained d_t^g [64] beyond saying it is consistent with zero.

Next we compare our results to the constraints listed below in Table II. For this purpose we have fixed M_S to 500 GeV, the parameters $\eta_{U,D} = 3$ and $\lambda_2 = 6$. The choice for mass is just a benchmark as there are no good limits on the masses of these type of scalars at the LHC [53]. The value for η_U is about tree times larger than the 1σ bound from R_b [41], and nearly 50% of its tree-level unitarity

TABLE II. Summary of results.

$m_t a_t^g$	$-2 \times 10^{-3} \lvert\frac{\eta_U}{3}\rvert^2 (\frac{500\ \mathrm{GeV}}{M_S})^2$
$m_t d_t^g$	$-8 \times 10^{-4} \lvert\frac{\eta_U}{3}\rvert^2 (\frac{500\ \mathrm{GeV}}{M_S})^2 (\frac{\lambda_2}{6}) \cos\alpha_U \sin\alpha_U$
$m_b a_b^g$	$-4.4 \times 10^{-6} \lvert\frac{\eta_{U,D}}{3}\rvert^2 (\frac{500\ \mathrm{GeV}}{M_S})^2$
$m_b d_b^g$	$-1.2 \times 10^{-6} \lvert\frac{\eta_{U,D}}{3}\rvert^2 (\frac{500\ \mathrm{GeV}}{M_S})^2 \sin(\alpha_D + \alpha_U)$
$m_t a_t^\gamma$	$-2 \times 10^{-3} \lvert\frac{\eta_U}{3}\rvert^2 (\frac{500\ \mathrm{GeV}}{M_S})^2$
$m_t d_t^\gamma$	$-1.4 \times 10^{-2} \lvert\frac{\eta_U}{3}\rvert^2 (\frac{500\ \mathrm{GeV}}{M_S})^2 (\frac{\lambda_2}{6}) \cos\alpha_U \sin\alpha_U$
$m_b a_b^\gamma$	$1.8 \times 10^{-6} \lvert\frac{\eta_{U,D}}{3}\rvert^2 (\frac{500\ \mathrm{GeV}}{M_S})^2$
$m_b d_b^\gamma$	$-1.2 \times 10^{-6} \lvert\frac{\eta_{U,D}}{3}\rvert^2 (\frac{500\ \mathrm{GeV}}{M_S})^2 \sin(\alpha_D + \alpha_U)$
f_T^R	$-2 \times 10^{-3} \lvert\frac{\eta_U}{3}\rvert^2 (\frac{500\ \mathrm{GeV}}{M_S})^2 e^{-2i\alpha_U}$

constraint [52]. Similarly, the benchmark chosen for λ_2 is well below its unitarity constraint [52] and at the level where it saturates the parameter S [38]. For example, keeping the values of $\eta_{U,D}$ and λ_2 fixed, the results in Table II can be used to interpret the bounds of Table I as constraints on M_S. The best LHC limit would be obtained from $\sigma(t\bar{t}h)$, $M_S \gtrsim 250$ GeV. Similarly the best overall limit, from the neutron edm, implies $M_S \gtrsim 316$ GeV. Both of these limits are slightly better than the existing robust LEP limit $M_S \gtrsim 100$ GeV [42]. A rough estimate for the production cross-section of a single $S^0_{R,I}$ with these masses can be found in [41,42,56], however, this cross section depends strongly on the parameters $\lambda_{4,5}$ which do not affect this work. Setting them to 1 results in $\sigma(S^0) \sim 2.7, 7.5$ pb for $M_S = 150, 500$ GeV respectively at LHC13[2] The main difference being that one of these values is above the $t\bar{t}$ threshold.

The SM one-loop result, $m_t a_t^g = -0.014$, is an order of magnitude larger than typical corrections predicted by this model, and is comparable to corrections in 2HDM or models with extra dimensions as computed in Ref. [3]. The corrections calculated here and listed in Table II are labeled "typical" as they can be pushed up by an order of magnitude by allowing couplings such as η_U to be as large as their unitarity upper bound and/or considering lighter scalars which at the moment are not ruled out.

Existing models with vector like multiplets [36] predict d_t^g as large as 0.003 a bit above our typical numbers. The range for d_t^g predicted in this model is below the reach of near future experiments, as are the b-quark couplings d_b^g and a_b^g.

The typical corrections to f_T^R in this model as shown in Table II are about a factor of three smaller than the SM one-loop value $f_T^R = -(7.17 + 1.23i) \times 10^{-3}$ as calculated in Ref. [32]. A major difference from results obtained in 2HDM [33] is that in the MW model the correction to f_T^R is much larger than that to f_T^L except for regions of parameter space where $\eta_U < \eta_D m_b/m_t$.

The typical values shown in Table II are below the potential constraints illustrated in Table I. But it is clear that as the experimental constraints approach the numbers in the Table, they will begin to limit the parameter space of the MW model beyond perturbative unitarity.

ACKNOWLEDGMENTS

R. M. was supported by El Patrimonio Autónomo Fondo Nacional de Financiamiento para la Ciencia, la Tecnología y la Innovación Francisco José de Caldas programme of COLCIENCIAS in Colombia. G. V. thanks the Departamento de Física, Universidad Nacional de Colombia for their hospitality while part of this work was completed.

APPENDIX: FEYNMAN PARAMETER INTEGRALS

All the loop diagrams appearing in the EDM, MDM, CEDM and CMDM calculations presented in this paper can be written in terms of the one parameter integrals

$$F_{n,m}(r) = \int_0^1 \frac{x^n(1-x)^m}{1-x+r^2x^2}dx$$
$$G_{n,m}(r_1,r_2) = \int_0^1 \frac{x^n(1-x)^m}{(1-x)(1-r_1^2x)+r_2^2x}dx. \quad \text{(A1)}$$

Although these integrals can be evaluated analytically, for the purposes of this paper we choose to evaluate numerically the combinations that appear in the final results. For convenience we present here the limiting values for small values of r, corresponding to large values of M_S.

$$F_{0,0}(r\to 0) = -4\log(r) - 3$$
$$F_{2,0}(r\to 0) = -2\log(r) - \frac{11}{6}$$
$$F_{3,0}(r\to 0) = -2\log(r) - \frac{3}{2}$$
$$F_{1,1}(r\to 0) = \frac{1}{2}$$
$$F_{1,2}(r\to 0) = \frac{1}{6}$$
$$F_{2,1}(r\to 0) = \frac{1}{3}$$
$$G_{n,m}(r_1\to 0, r_2\to 0) = F_{n,m}(r\to 0). \quad \text{(A2)}$$

For the calculation of f_T^R we need the two parameter Feynman integral

$$F_c(r_t,r_W) = \int_0^1 dx \int_0^{1-x} dy \frac{2y}{1-y+r_t^2y^2 - r_W^2 r_t^2 x(1-x) + r_t^2(1+r_W^2)xy}. \quad \text{(A3)}$$

Some manipulations have been carried out with the help of FeynCalc [65].

[2]We thank Alper Hayreter for providing these numbers.

[1] W. Buchmuller and D. Wyler, Effective Lagrangian analysis of new interactions and flavor conservation, Nucl. Phys. **B268**, 621 (1986).

[2] B. Grzadkowski, M. Iskrzynski, M. Misiak, and J. Rosiek, Dimension-six terms in the standard model Lagrangian, J. High Energy Phys. 10 (2010) 085.

[3] R. Martinez, M. A. Perez, and N. Poveda, Chromomagnetic dipole moment of the top quark revisited, Eur. Phys. J. C **53**, 221 (2008).

[4] Z. Hioki and K. Ohkuma, Optimal-observable analysis of possible non-standard top-quark couplings in $pp \to t\bar{t}X \to l^+X'$, Phys. Lett. B **716**, 310 (2012).

[5] Z. Hioki and K. Ohkuma, Latest constraint on nonstandard top-gluon couplings at hadron colliders and its future prospect, Phys. Rev. D **88**, 017503 (2013).

[6] J. Sjolin, LHC experimental sensitivity to *CP* violating g $t\bar{t}$ couplings, J. Phys. G **29**, 543 (2003).

[7] S. K. Gupta, A. S. Mete, and G. Valencia, *CP* violating anomalous top-quark couplings at the LHC, Phys. Rev. D **80** (2009) 034013.

[8] V. Barger, W. Y. Keung, and B. Yencho, Azimuthal correlations in top pair decays and the effects of new heavy scalars, Phys. Rev. D **85**, 034016 (2012).

[9] W. Bernreuther and Z. G. Si, Top quark spin correlations and polarization at the LHC: Standard model predictions and effects of anomalous top chromo moments, Phys. Lett. B **725**, 115 (2013); Corrigendum, Phys. Lett. B **744**, 413(E) (2015).

[10] S. S. Biswal, S. D. Rindani, and P. Sharma, Probing chromomagnetic and chromoelectric couplings of the top quark using its polarization in pair production at hadron colliders, Phys. Rev. D **88**, 074018 (2013).

[11] S. D. Rindani, P. Sharma, and A. W. Thomas, Polarization of top quark as a probe of its chromomagnetic and chromoelectric couplings in *tW* production at the Large Hadron Collider, J. High Energy Phys. 10 (2015) 180.

[12] A. Hayreter and G. Valencia, T-odd correlations from the top-quark chromoelectric dipole moment in lepton plus jets top-pair events, Phys. Rev. D **93**, 014020 (2016).

[13] N. Mileo, K. Kiers, A. Szynkman, D. Crane, and E. Gegner, Pseudoscalar top-Higgs coupling: Exploration of *CP*-odd observables to resolve the sign ambiguity, J. High Energy Phys. 07 (2016) 056.

[14] M. Baumgart and B. Tweedie, A new twist on top quark spin correlations, J. High Energy Phys. 03 (2013) 117.

[15] W. Bernreuther, D. Heisler, and Z. G. Si, A set of top quark spin correlation and polarization observables for the LHC: Standard Model predictions and new physics contributions, J. High Energy Phys. 12 (2015) 026.

[16] Z. Hioki and K. Ohkuma, Exploring anomalous top interactions via the final lepton in $t\bar{t}$ productions/decays at hadron colliders, Phys. Rev. D **83**, 114045 (2011).

[17] A. Hayreter and G. Valencia, Constraints on anomalous color dipole operators from Higgs boson production at the LHC, Phys. Rev. D **88**, 034033 (2013).

[18] J. Bramante, A. Delgado, L. Lehman, and A. Martin, Boosted Higgses from chromomagnetic *b*'s: $b\bar{b}h$ at high luminosity, Phys. Rev. D **93**, 053001 (2016).

[19] A. O. Bouzas and F. Larios, Electromagnetic dipole moments of the top quark, Phys. Rev. D **87**, 074015 (2013).

[20] M. Fischer, S. Groote, J. G. Korner, and M. C. Mauser, Complete angular analysis of polarized top decay at O(alpha (*s*)), Phys. Rev. D **65**, 054036 (2002).

[21] H. S. Do, S. Groote, J. G. Korner, and M. C. Mauser, Electroweak and finite width corrections to top quark decays into transverse and longitudinal *W* bosons, Phys. Rev. D **67**, 091501 (2003).

[22] J. A. Aguilar-Saavedra, J. Carvalho, N. F. Castro, A. Onofre, and F. Veloso, ATLAS sensitivity to Wtb anomalous couplings in top quark decays, Eur. Phys. J. C **53**, 689 (2008).

[23] J. A. Aguilar-Saavedra and J. Bernabeu, W polarisation beyond helicity fractions in top quark decays, Nucl. Phys. **B840**, 349 (2010).

[24] S. D. Rindani and P. Sharma, *CP* violation in tbW couplings at the LHC, Phys. Lett. B **712**, 413 (2012).

[25] B. Sahin and A. A. Billur, Anomalous Wtb couplings in gamma-proton collision at the LHC, Phys. Rev. D **86**, 074026 (2012).

[26] J. Ellis, V. Sanz, and T. You, Complete Higgs sector constraints on dimension-6 operators, J. High Energy Phys. 07 (2014) 036.

[27] C. Englert, A. Freitas, M. M. Mühlleitner, T. Plehn, M. Rauch, M. Spira, and K. Walz, Precision measurements of Higgs couplings: Implications for new physics scales, J. Phys. G **41**, 113001 (2014).

[28] C. Englert, D. Goncalves, and M. Spannowsky, Nonstandard top substructure, Phys. Rev. D **89**, 074038 (2014).

[29] V. Cirigliano, W. Dekens, J. de Vries, and E. Mereghetti, Is there room for *CP* violation in the top-Higgs sector?, Phys. Rev. D **94**, 016002 (2016).

[30] V. Cirigliano, W. Dekens, J. de Vries, and E. Mereghetti, Constraining the top-Higgs sector of the standard model effective field theory, Phys. Rev. D **94**, 034031 (2016).

[31] R. Martinez and J. A. Rodriguez, The anomalous chromomagnetic dipole moment of the top quark in the standard model and beyond, Phys. Rev. D **65**, 057301 (2002).

[32] G. A. Gonzalez-Sprinberg, R. Martinez, and J. Vidal, Top quark tensor couplings, J. High Energy Phys. 07 (2011) 094; Erratum, J. High Energy Phys. 05 (2013) 117(E).

[33] L. Duarte, G. A. González-Sprinberg, and J. Vidal, Top quark anomalous tensor couplings in the two-Higgs-doublet models, J. High Energy Phys. 11 (2013) 114.

[34] R. Gaitan, E. A. Garces, J. H. M. de Oca, and R. Martinez, Top quark chromoelectric and chromomagnetic dipole moments in a two Higgs doublet model with *CP* violation, Phys. Rev. D **92**, 094025 (2015).

[35] A. Arhrib and A. Jueid, *tbW* anomalous couplings in the two Higgs doublet model, J. High Energy Phys. 08 (2016) 082.

[36] T. Ibrahim and P. Nath, The chromoelectric dipole moment of the top quark in models with vector like multiplets, Phys. Rev. D **84**, 015003 (2011).

[37] A. Aboubrahim, T. Ibrahim, P. Nath, and A. Zorik, Chromoelectric dipole moments of quarks in MSSM extensions, Phys. Rev. D **92**, 035013 (2015).

[38] A. V. Manohar and M. B. Wise, Flavour changing neutral currents, an extended scalar sector, and the Higgs production rate at the CERN LHC, Phys. Rev. D **74**, 035009 (2006).

[39] R. S. Chivukula and H. Georgi, Composite technicolour standard model, Phys. Lett. B **188**, 99 (1987).
[40] G. D'Ambrosio, G. F. Giudice, G. Isidori, and A. Strumia, Minimal flavour violation: An effective field theory approach, Nucl. Phys. **B645**, 155 (2002).
[41] M. I. Gresham and M. B. Wise, Colour octet scalar production at the LHC, Phys. Rev. D **76**, 075003 (2007).
[42] C. P. Burgess, M. Trott, and S. Zuberi, Light octet scalars, a heavy Higgs and minimal flavour violation, J. High Energy Phys. 09 (2009) 082.
[43] X.-G. He and G. Valencia, An extended scalar sector to address the tension between a fourth generation and Higgs searches at the LHC, Phys. Lett. B **707**, 381 (2012).
[44] B. A. Dobrescu, G. D. Kribs, and A. Martin, Higgs underproduction at the LHC, Phys. Rev. D **85**, 074031 (2012).
[45] Y. Bai, J. Fan, and J. L. Hewett, Hiding a heavy Higgs boson at the 7 TeV LHC, J. High Energy Phys. 08 (2012) 014.
[46] G. Cacciapaglia, A. Deandrea, G. D. La Rochelle, and J.-B. Flament, Higgs couplings beyond the standard model, J. High Energy Phys. 03 (2013) 029.
[47] J. Cao, P. Wan, J. M. Yang, and J. Zhu, The SM extension with colour-octet scalars: diphoton enhancement and global fit of LHC Higgs data, J. High Energy Phys. 08 (2013) 009.
[48] X. G. He, Y. Tang, and G. Valencia, Interplay between new physics in one-loop Higgs couplings and the top-quark Yukawa coupling, Phys. Rev. D **88**, 033005 (2013).
[49] B. Grinstein, A. L. Kagan, J. Zupan, and M. Trott, Flavor symmetric sectors and collider physics, J. High Energy Phys. 10 (2011) 072.
[50] X. D. Cheng, X. Q. Li, Y. D. Yang, and X. Zhang, $B_{s,d} - \bar{B}_{s,d}$ mixings and $B_{s,d} \to \ell^+\ell^-$ decays within the Manohar-Wise model, J. Phys. G **42**, 125005 (2015).
[51] M. Reece, Vacuum instabilities with a wrong-sign Higgs-gluon-gluon amplitude, New J. Phys. **15**, 043003 (2013).
[52] X. G. He, H. Phoon, Y. Tang, and G. Valencia, Unitarity and vacuum stability constraints on the couplings of colour octet scalars, J. High Energy Phys. 05 (2013) 026.
[53] L. Cheng and G. Valencia, Two Higgs doublet models augmented by a scalar colour octet, J. High Energy Phys. 09 (2016) 079.
[54] M. Gerbush, T. J. Khoo, D. J. Phalen, A. Pierce, and D. Tucker-Smith, Colour-octet scalars at the CERN LHC, Phys. Rev. D **77**, 095003 (2008).
[55] J. M. Arnold and B. Fornal, Colour octet scalars and high pT four-jet events at LHC, Phys. Rev. D **85**, 055020 (2012).
[56] X.-G. He, G. Valencia, and H. Yokoya, Colour-octet scalars and potentially large *CP* violation at the LHC, J. High Energy Phys. 12 (2011) 030.
[57] G. D. Kribs and A. Martin, Enhanced di-Higgs production through light coloured scalars, Phys. Rev. D **86**, 095023 (2012).
[58] J. F. Kamenik, M. Papucci, and A. Weiler, Constraining the dipole moments of the top quark, Phys. Rev. D **85**, 071501 (2012); Erratum, Phys. Rev. D **88**, 039903(E) (2013).
[59] B. Grzadkowski and M. Misiak, Anomalous Wtb coupling effects in the weak radiative B-meson decay, Phys. Rev. D **78**, 077501 (2008); Erratum, Phys. Rev. D **84**, 059903(E) (2011).
[60] R. Martinez and J. A. Rodriguez, Constraint of the magnetic moment of the top quark from R(b), Phys. Rev. D **60**, 077504 (1999).
[61] Z. Hioki and K. Ohkuma, Full analysis of general non-standard tbW couplings, Phys. Lett. B **752**, 128 (2016).
[62] Z. Hioki, K. Ohkuma, and A. Uejima, Refined analysis and updated constraints on general non-standard *tbW* couplings, Phys. Lett. B **761**, 219 (2016).
[63] V. Khachatryan *et al.* (CMS Collaboration), Search for anomalous Wtb couplings and flavour-changing neutral currents in t-channel single top quark production in pp collisions at sqrt(s) = 7 and 8 TeV, arXiv:1610.03545.
[64] CMS Collaboration, Report No. CMS-PAS-TOP-16-001.
[65] R. Mertig, M. Böhm, and A. Denner, Feyn Calc - Computer-algebraic calculation of Feynman amplitudes, Comput. Phys. Commun. **64**, 345 (1991); V. Shtabovenko, R. Mertig, and F. Orellana, New developments in FeynCalc 9.0, Comput. Phys. Commun. **207**, 432 (2016).